Optimization of the Selection of Hidden Particles in the SHiP Experiment

Guilherme Machado Santos Soares
Under supervision of Celso Franco and Nuno Leonardo
Laboratório de Instrumentação e Física Experimental de Partículas, Instituto Superior Técnico, Lisboa, Portugal
(Dated: January 2021)

Although the Standard Model is one of the biggest achievements in physics, it cannot explain several outstanding phenomena, such as the existence of Dark Matter. The SHiP experiment will try to discover Hidden Sector particles that solve some shortcomings, through the direct observation of at least two decays to the SM, requiring several background veto systems. These prospects include Heavy Neutral Leptons and Dark Photons. We suggest several optimized background veto criteria for the SHiP experiment utilizing the kinematic properties of the reconstructed particles, regarding Heavy Neutral Leptons in the mass range between 0.7 and 1.4 GeV/c^2, and Dark Photons in the mass range between 0.021 and 4.4 GeV/c^2, by using a cut-based approach and machine learning methods. Additionally, we discuss the relaxation of the Decay Vessel vacuum conditions to an air pressure of 1 bar.
Keywords: Search for Hidden Particles Experiment; Heavy Neutral Leptons; Dark Photons; Selection Efficiencies; Background Rejection Studies.

I. INTRODUCTION

The Standard Model (SM) is one of the biggest accomplishments in physics up to this date. It describes all the known elementary particles and their interactions, with very high precision at energies up to the TeV scale. In spite of this, the SM is not perfect and there are some shortcomings, that range from big theoretical gaps such as the unavailability of a Dark Matter (DM) candidate, to more precise problems such as possible small violations of the constructed leptonic flavour universality [1].

The Search for Hidden Particles experiment (SHiP) [2] is a proposed fixed target experiment to be set at the SPS accelerator at CERN, and one of its main goals is to search for physics Beyond the SM (BSM) in the Hidden Sector (HS). Two of the HS particles that will be probed at SHiP will be Heavy Neutral Leptons (HNLs) [3] and DarkPhotons (DPs) [4]. HNLs are massive right-handed neutrinos that do not couple to the weak force, and consequently to no force in the SM. Within a specific range of the parameter space, they are able to solve the SM neutrino mass problem, provide a DM candidate, and alongside inflatons might be able to generate the baryonic asymmetry of the universe [5]. DPs are massive gauge bosons that mix with SM photons, and are associated with a new $U(1)_D$ symmetry that applies to HS fermions, but not to SM ones. They provide a self-annihilation mechanism into the SM for DM, and might be themselves a DM candidate. Apart from this, their detection heavily implies the existence of a larger HS [6].

To detect these particles, SHiP will need the direct observation of at least two decays of said particles into SM products. This requires the existence of several background veto systems, and sub-optimal selection of the HS events can compromise the sensitivity of the experiment. We will present background veto criteria that optimize the selection of DPs and HNLs at SHiP, using the kinematic features of the particles reconstructed in the Hidden Sector Spectrometer. This will be done through a cut-based analysis and Machine Learning (ML) methods. Additionally, we explore the extreme case where the Decay Vessel is filled with air at a pressure of 1 bar, instead of the currently planned 1 mbar.

II. THE SHIP EXPERIMENT

The particles that SHiP will search for are expected to be predominantly accessible through the decays of heavy hadrons. The facility is therefore designed to maximise the production and detector acceptance of charm and beauty mesons, while providing the cleanest possible environment. The 400 GeV proton beam extracted from the SPS will be dumped on a high density target with the aim of accumulating 2×10^{20} protons on target during 5 years of operation. The charm production at SHiP exceeds any existing and planned facility.

A dedicated detector, based on a long vacuum tank followed by a spectrometer and particle identification detectors, will allow probing a variety of models with light long-lived exotic particles and masses below $\mathcal{O}(10)$ GeV/c^2.

A critical component of SHiP is the muon shield, which deflects the high flux of muons produced in the target away from the detector, that would represent a serious background for the particle searches. The detector is designed to fully reconstruct the exclusive decays of hidden particles and to reject the background down to below 0.1 events in the sample of 2×10^{20} protons on target. The detector consists of a large magnetic straw spectrometer located downstream of a 50 m-long and 5×10 m-wide decay vessel. To suppress the background from neutrinos interacting in the fiducial volume, the decay volume is maintained under a vacuum. The spectrometer is designed to accurately reconstruct the decay vertex, mass and impact parameter of the decaying particle at the tar-

get. A set of calorimeters followed by muon chambers provide identification of electrons, photons, muons and charged hadrons. A dedicated timing detector measures the coincidence of the decay products, which allows the rejection of combinatorial backgrounds. The decay volume is surrounded by background taggers to tag neutrino and muon inelastic scattering in the surrounding structures, which may produce long-lived SM V^0 particles, such as K_L, that have similar topologies to the expected signals.

The experimental facility is also ideally suited for studying interactions of tau neutrinos. It will therefore host an emulsion cloud chamber based on the Opera concept, upstream of the hidden-particle decay volume, followed by a muon spectrometer.

III. EXTENSIONS OF THE STANDARD MODEL

A. Heavy Neutral Leptons

HNLs are massive right-handed $SU(2)_L \times U(1)_Y$ singlets that couple to the SM through their left-handed SM counterparts. The Neutrino Minimal Standard Model (νMSM) is an extension to the SM that includes three HNLs with masses below the electroweak scale [7]. As mentioned previously, this model is able to provide a DM candidate, explain neutrino masses and provide a leptogenesis mechanism to create the baryonic asymmetry of the universe (BAU), making HNLs of the utmost interest at SHiP.

The most general gauge invariant interactions can be described by the following Lagrangian extension:

$$\mathcal{L}_N = \overline{N}_I i\partial_\mu \gamma^\mu N_I - \left[F_{\alpha I} \overline{\ell_\alpha} N_I \tilde{\Phi} + \frac{M_I}{2} \overline{N}_I^c N_I + \text{H.c.} \right], \quad (1)$$

where N_I are the HNL singlets with $I = (1, 2, 3)$, Φ is the Higgs doublet, ℓ_α are the SM lepton doublets with $\alpha = (e, \mu, \tau)$, and $F_{\alpha I}$ is a 3×3 complex matrix that provides Yukawa-like couplings. Notice that it is implied that the SM lepton doublets are left-handed, while the new HNLs are right-handed. It is also worthy to mention that we are considering the Sterile Neutrinos to be Majorana particles, with a Majorana mass term M_I, since they do not have the need to conserve the SM lepton number. This extension is well known, from seesaw mechanisms, and is able to explain the observed SM neutrino masses through the PMNS mixing matrix [8]. This leads to an effective model where the HNLs kinetically mix with the SM neutrinos through their effective couplings $|U_{\alpha I}|^2$, and as such interact with SM particles in the same fashion as standard neutrinos, albeit suppressed by a factor of $|U_{\alpha I}|^2$.

If we follow Ref. [9], by requiring that the lightest HNL be the DM candidate, and that the two heaviest are almost degenerate in mass and have sizeable couplings to the SM neutrinos $F_{\alpha I}$, creating the mechanism responsible for BAU, then $|U_{\alpha 2}|^2 \simeq |U_{\alpha 3}^2| \equiv |U_\alpha|^2$. Additionally, by requiring that the SM lepton flavour universality be slightly broken, we are able to derive ratios between these couplings, leading to three benchmark models utilized in SHiP related studies:

$$\begin{aligned} \text{model I:} \quad & U_e^2 : U_\mu^2 : U_\tau^2 \approx 52 : 1 : 1, \quad \kappa = 2, \\ \text{model II:} \quad & U_e^2 : U_\mu^2 : U_\tau^2 \approx 1 : 16 : 3.8, \quad \kappa = 1, \\ \text{model III:} \quad & U_e^2 : U_\mu^2 : U_\tau^2 \approx 0.061 : 1 : 4.3, \quad \kappa = 1, \end{aligned}$$

where $\kappa = (1, 2)$ stands for the normal and inverted hierarchies of neutrino masses, respectively, and $|U_\alpha|^2 \equiv U_\alpha^2$ for simplicity. This model gives us an experimental signature of HNLs that only depends on their masses $M_2 \simeq M_3 \equiv M_N$, and the three mixing parameters $|U_\alpha|^2$.

B. Dark Photons

The DPs are massive gauge bosons associated with a BSM $U(1)_D$ symmetry. These theories are very well motivated, since breaking symmetry groups with high ranks often leads to the creation of several low energy $U(1)$ symmetries. As such, it is not as important to know how a DP might be created[1], but rather its phenomenological implications. Regardless of the high-energy theory that originates the DP, if it is to couple to the SM, it is always through kinetic mixing with the bosons of the $U(1)_Y$ symmetry of the SM [11].

The easiest way of adding a Dark Photon to the currently existing paradigm does not include direct couplings to the SM particles. Given that, the simplest extension to the Lagrangian is the following:

$$\mathcal{L}_{A'} = -\frac{1}{4} \left(F'_{\mu\nu} \right)^2 - \frac{\epsilon}{2} F'_{\mu\nu} F^{\mu\nu} - \frac{1}{2} m_{\gamma_D}^2 \left(A'_\mu \right)^2 . \quad (2)$$

Here $F^{\mu\nu}$ is the SM $U(1)_e$ field strength, given by $F_{\mu\nu} = \partial_\mu F_\nu - \partial_\nu F_\mu$, $F'_{\mu\nu}$ is the field strength of the Dark Photon with an analogous definition, ϵ is the mixing factor and m_{γ_D} is the mass of the Dark Photon. Analogously to the HNLs, the mixing factor ϵ provides interactions of the DP with the SM equal to those of the SM photon, albeit suppressed. As such, the DP experimental signature can be defined by just two parameters: the mixing parameter ϵ and the DP mass m_{γ^D}.

IV. SAMPLES AND SIMULATION

In the simulation, proton fixed target collisions are generated by PYTHIAv8 [12], inelastic neutrino interactions by GENIE [13] and inelastic muon interactions by

[1] For a more comprehensive look into the implications of new $U(1)'$ symmetries see Ref. [10].

PYTHIA6 [14]. The heavy flavour cascade production is also taken into account [15]. The SHiP detector response is simulated in the GEANT4 [16] framework. The simulation is done within the FAIRROOT framework [17]. The pattern recognition of the Spectrometer Straw Tracker can be seen in Ref. [18], and the algorithms for particle identification are in Ref. [19].

Even though the samples generated for the background have different selection criteria according to the signal that is being studied, a simple preliminary cut is always applied. We always have to ensure that the HS candidate particle was reconstructed inside the decay vessel, with a cutoff of the fiducial volume at 5 cm from any walls.

A. Background

As stated previously, the SHiP facility will be a charm and beauty meson factory. The compromise to having a large enough amount of these mesons is the associated high amount of light mesons, muons and SM neutrinos produced. While the light mesons are innocuous due to the hadronic shield, the muons cannot be totally deflected and the neutrinos cannot be deflected at all, thus creating the main background sources for the studies related to the detection of HS particles. In the case of muons, performing inelastic scattering interactions with the apparatus can produce long-lived neutral hadrons just before the decay vessel. As for neutrinos, apart from a similar problem to the muons, DIS interactions can also create meaningful background inside the vessel, since unlike the muons we cannot detect them when they enter the volume, and veto the event.

While an unparalleled amount of both τ flavoured neutrinos and anti-neutrinos will be produced at SHiP, naturally the amount is much inferior to that of electron and muon flavoured ones. Thus, the neutrino DIS background studies only considered the latter flavours. This lead to generating 1.0×10^6 electron and muon flavoured neutrino and anti-neutrino DIS interactions in the SHiP apparatus, with interactions forced to occur between the beginning of the muon ID system upstream of the decay vessel, until the second target tracker of the straw spectrometer. As for the muon generated background, a total of $\approx 1.0 \times 10^6$ DIS interactions were forced within the same range as the neutrino ones.

Additionally, approximately 2.18×10^9 events of what is considered the random muon combinatorial background were generated. This background consists of unrelated muons that are detected by the apparatus, which then recreates an artificial vertex inside the decay vessel. However, these events rarely mimic HS topologies and their background potential stems from their sheer volume. This leads to very low reconstruction efficiencies, and a statistically significant study could not be done from this source.

A summary of the generated background events and their preliminary cuts can be seen in Table I.

Background	Events Generated	Particles Reconstructed (inside the Decay Vessel)
ν_e DIS	1.0×10^6	16804 (7741)
$\overline{\nu_e}$ DIS	1.0×10^6	11653 (5959)
ν_μ DIS	1.0×10^6	4913 (1807)
$\overline{\nu_\mu}$ DIS	1.0×10^6	2986 (1046)
μ DIS	1.0325×10^6	10511 (3015)
μ Comb.	2.18×10^9	4 (3)

TABLE I. Summary of the background samples generated with the **FairShip** software. Particles reconstructed take into account a combination of at least 2 tracks. μ Comb. stands for the muon combinatorial background.

B. Hidden Sector

Several sensitivity studies of the SHiP experiment to the HS particles that will be probed have been performed. The most recent ones regarding HNLs and DPs can be seen in Refs. [20] and [21], and were utilized as references when choosing the mass/coupling pairings for the HS samples. In this study several points of the parameter space were considered, as well as the most relevant decay modes for the regions of interest. Since selection inefficiencies are more damaging near the sensitivity limits, save a few exceptions, all couplings selected were near said limits. The sensitivity limit was established at > 2.4 expected events over the full operational time of the experiment, so to get a significant statistical sample, 5000 events were generated for each point selected.

Following Ref. [20], SHiP will have its best sensitivity to HNLs around a mass of 1 GeV/c^2. As stated in studies relating to the νMSM [5], the masses preferred in order to create a Dark Matter candidate while also providing a viable mechanism to explain BAU are of the order of 1 GeV/c^2. Accordingly samples were generated for masses that range from 0.7 to 1.4 GeV/c^2, in 0.1 GeV/c^2 intervals. For masses smaller than $m_D \approx 1.9$ GeV/c^2, the biggest source of production of HNLs is the decay of charmed mesons. As such all HNL samples were produced from open charm mesons. The most relevant decays were considered, and additionally an effort was done to include samples that have decay products that cannot be fully detected, and lead to missing energy in the reconstructions. This lead to creating the following samples: $N \to e^\mp \pi^\pm$, $N \to \mu^\mp \pi^\pm$, $N \to e^\mp \rho^\pm$, $N \to \mu^\mp \rho^\pm$, $N \to \nu_\alpha \mu^\pm \mu^\mp$ and $N \to \nu_\alpha \rho^0$, with $\alpha = e, \mu, \tau$. As was mentioned in Section III, there are three benchmark models for HNLs at SHiP, so for each selected point of the parameter space, three samples corresponding to the three models were generated. A summary of the HNL parameter space is presented in Table II.

The probing capability of SHiP for DPs has a cigar shape, and both the upper and lower bounds, coupling-wise, are of interest. One of the big implications of DPs is the shift in the magnetic dipole of the muon. Solutions to

Mass [GeV/c^2]	Maximum Coupling $\|U_\alpha\|^2$	
	Models I, II	Model III
0.7*	1.2×10^{-9}	4×10^{-9}
0.8*	9×10^{-10}	2.4×10^{-9}
0.9	6×10^{-10}	1.8×10^{-9}
1.0	5×10^{-10}	1.2×10^{-9}
1.1	3×10^{-10}	9×10^{-10}
1.2	2.5×10^{-10}	7×10^{-10}
1.3	2.0×10^{-10}	6×10^{-10}
1.4	1.8×10^{-10}	4×10^{-10}

TABLE II. Maximum couplings selected for each HNL mass and benchmark model. *No simulations involving decays with ρ particles were done for masses lower than 0.9 GeV/c^2.

the muon g-2 anomaly involving DPs are disfavoured for masses $m_{\gamma^D} > 400$ MeV/c^2 [22, 23]. This lead to selecting masses under 400 MeV/c^2 within small intervals. As for bigger masses, intervals of ≈ 1 GeV/c^2 were chosen in order to complete the sweep, up until 4.4 GeV/c^2 [2]. Table III includes the detailed masses utilized when generating the samples alongside the couplings provided. For some masses two couplings were selected, since there is both a lower and upper bound based on the minimum 2.4 expected events. Due to the reduced physical relevance for masses that surpass 1 GeV/c^2, and also due to the naturally shrinking range of couplings for such masses, only one centralized coupling was provided for 3.6 and 4.4 GeV/c^2. DPs have three main production modes at SHiP. For masses smaller than 0.5 GeV/c^2 meson decays are the dominant process, while for masses larger than 1.4 GeV/c^2 direct QCD production is more relevant [21]. As for the decay modes, at low enough masses of $m_{\gamma_D} \leq 2m_\mu$, the only available decay mode into SM particles is $A' \to e^- e^+$. For masses in the range $2m_\mu \leq m_{\gamma_D} \leq 2m_\pi \approx 400$ MeV/c^2, which encompasses the remaining area of very high interest, the only other SM decay channel that opens up is $A' \to \mu^- \mu^+$. As such, these two decay channels were the only ones studied.

Table IV summarizes the HS samples, and shows the number of particles that were reconstructed inside the decay vessel.

Mass [MeV/c^2]	Effective Coupling ε	Mass [MeV/c^2]	Effective Coupling ε
21	1.0×10^{-4}	200	1.0×10^{-5}
30	7×10^{-5}		8×10^{-8}
40	6×10^{-5}	250*	1.0×10^{-5}
50	4.4×10^{-5}		5×10^{-8}
60	4.0×10^{-5}	500*	3.0×10^{-6}
70	4.0×10^{-5}		4.0×10^{-8}
80	3.0×10^{-5}	1400*	1.0×10^{-6}
90	2.4×10^{-5}		5×10^{-8}
100	2.0×10^{-5}	2500*	3.0×10^{-7}
120	2.0×10^{-5}		5×10^{-8}
140	2.0×10^{-5}	3600*	5×10^{-8}
160	1.4×10^{-5}	4400*	5×10^{-8}
180	1.4×10^{-5}	–	–

TABLE III. Detailed masses chosen for the Dark Photon simulations, and respective couplings selected for each. Notice that for a mass of 500 MeV/c^2, there are two different couplings. *The channel $A' \to \mu^+ \mu^-$ is only open for masses of 250 MeV/c^2 or higher.

Decay Mode	Events Generated	Particles Reconstructed (inside the Decay Vessel)
$N \to e^- \pi^+$	1.2×10^5	26307 (25116)
$N \to \mu^- \pi^+$	1.2×10^5	28338 (26867)
$N \to e^- \rho^+$	9.0×10^4	23226 (21923)
$N \to \mu^- \rho^+$	9.0×10^4	25994 (24235)
$N \to \nu_\alpha \mu^+ \mu^-$	1.2×10^5	30800 (29001)
$N \to \nu_\alpha \rho^0$	9.0×10^4	22781 (21373)
$A' \to e^- e^+$	1.25×10^5	34810 (33324)
$A' \to \mu^- \mu^+$	5.0×10^4	17667 (16954)

TABLE IV. Summary of the HS samples generated with the **FairShip** software. Decay modes involving ρ particles were only simulated for HNLs with masses of 0.9 GeV/c^2 or higher. The decay to a pair of muons was only simulated for DPs with masses of 250 MeV/c^2 or higher. Notice that the charge conjugate channels are also included.

V. CUT-BASED STUDY

Even though preliminary studies were done on the background and its sources, as can be seen as far back as the Technical Proposal [2], which provide a standard set of cuts able to reduce the background to the accepted levels, taking into account the use of physical veto systems, it was done for the preliminary configuration of the SHiP apparatus, which as since been heavily altered. More recent studies have been done, and a summary can be seen in the latest Comprehensive Design Study Report [24]. However this latter study also takes into account the use of physical veto systems, and as such runs parallel to our own.

Unlike for the first study, we do not have access to precise numbers on the amount of background events expected throughout the whole experiment, and as such we

[2] At the time of the sample generation the most recent sensitivity study was not available yet, reducing the probing range to $\mathcal{O}(3)$GeV/c^2.

will not be able to define cuts based on a clear cut-off of 0.1 events expected over the whole experiment. This lead to the decision of making unorthodox cuts that remove every single background event, regardless of their significance. With this said, we shall proceed to explain the cuts applied, as well as their reasoning, and the results obtained.

The first cut applied after the preliminary one was to only accept reconstructions that came from specific sets of particles that could be generated by the HS particles. Afterwards, since the FAIRROOT algorithm did not reconstruct automatically neutral pions at the time of the study, we searched for those. With this, we then proceeded to analyse the kinematic properties of the reconstructed HS candidate particle, as well as of the particles that interacted with the detector, leading to the set of features presented in Table V. If a neutral pion was found, it was taken into consideration for the features related to the reconstructed HS candidate particle. From here on out, we will refer to the HS candidate as Mother and to the particles that interacted with the detectors as tracks.

Feature	Symbol
Total Momentum	TotMom
Transverse Momentum	TransMom
Fraction of Transverse Momentum	FracMom
Opening Angle	OA
Impact Parameter	IP
Coordinates of the Decay Vertex	Decay X, Y and Z

TABLE V. Kinematic features extracted from the reconstructed particles, and respective symbols that will be utilized when describing the kinematic cuts. When considering the coordinates of the decay vertex Z relates to the initial proton beam axis, while X and Y are the transverse coordinates.

The distributions of these features were compared between the HS signal and the background, and a set of loose preliminary cuts was established around the features that showed the most significant differences. Whether for HNLs or DPs, these were the IP, the TotMom of the Mother and the Decay Z. The distribution of the IP from all the HNL samples combined (blue) against the background (orange), can be seen in Fig. 1. After the preliminary set of cuts, all the combinations of two variables available were compared in order to find cuts that could remove every single background event. In order to optimize these cuts, in the end, every single cut was individually removed, and new cut thresholds were sought for the cut, such that the selection efficiency of the HS samples was as high as possible, while maintaining the 0 background events selected.

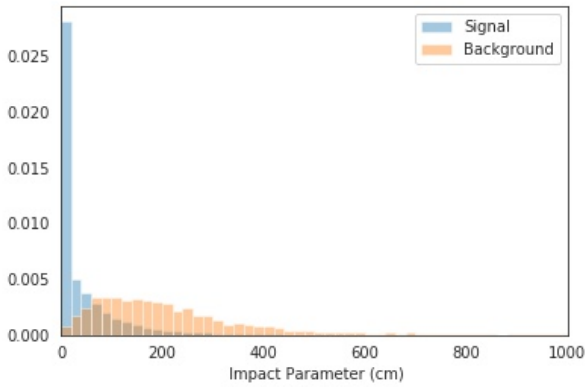

FIG. 1. Distributions of the Impact Parameter for all the HNL samples combined (blue) and for the respective background (orange). Both distributions are normalized so that the integral yields ≈ 1.

A. Heavy Neutral Leptons

All of the decay modes selected for the HNLs effectively have as final products combinations of pions and light leptons, indeed the ρ particles decay fairly quickly into pairs of pions, be it $\rho^{\pm} \to \pi^{\pm}\pi^{0}$ or $\rho^{0} \to \pi^{-}\pi^{+}$. As such we only accept HS events if their tracks belonged to the following combinations:

$$e^{\mp}\pi^{\pm},\ \mu^{\mp}\pi^{\pm},\ \pi^{\mp}\pi^{\pm},\ e^{\mp}\mu^{\pm} \text{ or } \mu^{\mp}\mu^{\pm}, \tag{3}$$

where $e^{\pm}\mu^{\mp}$ takes into account misidentifications of charged pions. The reconstruction algorithm in **FairShip** at the time of the analysis did not reconstruct neutral pions automatically from photons. The cuts regarding the kinematic features can be found in Table VI, and the selection efficiencies obtained by cut are detailed in Table VII. Final selection efficiencies broken down by decay mode can be found in Table X, alongside the DPs. From this breakdown two things stand out: while the simpler decays $N \to \ell^{\mp}\pi^{\pm}$ have very acceptable selection efficiencies, the decays with missing energy in the form of SM neutrinos have low ones. This very high contrast stems from the fact that most of the cuts were based around the Impact Parameter, which does seem to be a very good distinguishing feature. The drawback to this approach is that most of its strength lies on the fact that neutrino and muon DIS events are usually reconstructed with either missing energy or off the beam axis, since the Impact Parameter is calculated by propagating the reconstructed HS particle (mother) to the point where it is expected to have been created, at the SHiP target, and measuring the closest distance. This leads to very low selection efficiencies for decays that cannot be fully reconstructed due to their undetectable decay products.

Cut	Thresholds for Selection
1	IP < 33.0 cm.
2	TotMom of the Tracks > 1.0 GeV/c.
3	IP > 6.0 or > 10.0 cm requires TotMom of the Mother < 58.0 or 38.0 GeV/c, respectively.
4	IP > 12.0 or 16.0 cm requires TransMom of the Track < 0.25 GeV/c or > 1.45 GeV/c, respectively.
5	IP < 12.0 cm requires IP $< 412 \times (0.05 - \text{TransMom})^2 + 2.0$ cm, where TransMom is from the Tracks, in GeV/c.
6	IP $< 47043 \times (0.0005 - \text{FracMom})^2 + 2.0$ cm, where FracMom is from the Mother in GeV/c.
7	Decay Z > 35.3 cm.

TABLE VI. Kinematic cuts applied to the HNL samples, and their respective background.

Cut	Background Events Selected (%)	HNL Events Selected (%)
PID	4828 (24.7)	143742 (96.8)
1	171 (0.9)	90574 (61.0)
2	137 (0.7)	89456 (60.2)
3	81 (0.4)	76219 (51.3)
4	26 (0.1)	73234 (49.3)
5	18 (0.1)	69898 (47.1)
6	5 (0.0)	64796 (43.6)
7	0 (0.0)	64633 (43.5)

TABLE VII. Selection efficiency of the kinematic cuts from Table VI. The PID cut refers to the combinations of tracks presented in Eq. (3). All percentages are calculated against the total number of HS candidate particles reconstructed within the decay vessel, which gives a total of 19568 background events, and 148515 HNL events.

B. Dark Photons

The only decay modes studied for the Dark Photons were the decays into pairs of charged leptons. So, the first cut applied after the preliminary ones was to only consider combinations of muons and electrons, which correspond to the next three combinations:

$$e^- e^+,\ \mu^- \mu^+ \text{ and } e^{\mp}\mu^{\pm}. \tag{4}$$

Even though there are no decays involving neutral pions, we still searched for them, since they should not appear in our signal samples this time around, providing a good veto for background events. As mentioned previously, the sensitivity limits were updated recently, and as such this study included some DP samples with masses that most likely will not be able to be probed at SHiP. We will therefore also present the selection efficiencies of the cuts applied on a sample of Dark Photons that does not take into account events with masses of 3.6 and 4.4 GeV/c^2.

The cuts regarding the kinematic features can be found in Table IX and the selection efficiencies obtained by cut are detailed in Table VIII. Final selection efficiencies broken down by decay mode can be found in Table X. As was expected, the selection efficiencies are very high for the Dark Photons, reaching $\approx 95\%$ for the muonic decay channel within the most recent sensitivity estimates, even though the Impact Parameter cut was tightened. Once again, decay channels involving muons are favoured in comparison with their electron counterparts, which is natural, since the muons tend to interact much less with the environment, and usually produce clearer experimental signatures.

Cut	Background Events Selected (%)	DP Events Selected (%)
PID	6806 (34.8)	50209 (99.9)
1	120 (0.6)	47982 (95.4)
2	25 (0.1)	47048 (93.6)
3	22 (0.1)	46515 (92.5)
4	7 (0.0)	45742 (91.0)
5	4 (0.0)	44803 (89.1)
6	3 (0.0)	44773 (89.1)
7	0 (0.0)	44082 (87.7)

TABLE VIII. Selection efficiency of the kinematic cuts from Table IX. The PID cut refers to the combinations of tracks presented in Eq. (4). All percentages are calculated against the total number of HS candidate particles reconstructed within the decay vessel, which gives a total of 19568 background events and 50278 DP events.

VI. MACHINE LEARNING

Machine Learning (ML) algorithms provide very bright prospects for analysing data sets, since they can compare the information taking into account multi-variable

Cut	Thresholds for Selection
1	IP < 27.0 cm.
2	IP $< 8.7 \times (0.466 - \text{TotMom})^2 + 6.5$ cm, where TotMom is from the Tracks in GeV/c.
3	IP > 14.8 or 23.7 cm requires TotMom of the Mother < 66.0 or 47.0 GeV/c, respectively.
4	IP > 10.15 cm requires IP $< 168.87 \times$ TransMom $- 3.41$ cm, where TransMom is from the Tracks in GeV/c.
5	IP $< 50484 \times (0.0012 - \text{TransMom})^2 + 1.79$ cm, where TransMom is from the Tracks, in GeV/c.
6	IP > 6.15 cm requires OA > 0.0026 rad.
7	Decay Z > 156.0 cm.

TABLE IX. Kinematic cuts applied to the DP samples, and their respective background.

Decay Mode	Surviving Events after the Cuts (%)
$N \to e^- \pi^+$	20417 (81.3)
$N \to \mu^- \pi^+$	24524 (91.3)
$N \to e^- \rho^+$	7729 (36.5)
$N \to \mu^- \rho^+$	9494 (39.2)
$N \to \nu_\alpha \mu^+ \mu^-$	1054 (3.6)
$N \to \nu_\alpha \rho^0$	1415 (6.6)
$A' \to e^- e^+$	27981 (84.0)
$A' \to \mu^- \mu^+$	16101 (95.0)
$^*A' \to e^- e^+$	25608 (84.7)
$^*A' \to \mu^- \mu^+$	13253 (95.1)

TABLE X. Summary of the selection efficiency obtained for the HS samples by applying their respective kinematic cuts, detailed by decay mode. Efficiencies are based on the HS candidate particles reconstructed within the decay vessel. *Dark Photon events without the 3.6 and 4.4 GeV/c^2 mass samples, that are not within the most recent sensitivity estimates.

correlations that are non-trivial. Their use has become quite frequent nowadays, including for what regards selection or classification problems such as the namesake of this thesis [25]. In this case, a set of Multilayer Perceptrons (MLPs) was utilized. These are Neural Networks (NN) with non-linear activation functions. For the implementation of our algorithms we used Keras [26], an open-source library that provides a Python interface for artificial neural networks. Keras acts as an interface for the TensorFlow [27] library.

The first step taken in order to apply Neural Networks to the data was to normalize all features to the same scale, in order to prevent unwanted biases revealed during the validation of the network. This was done by applying a standard scaler to all features fed onto the network, which transforms the whole set so that the mean value is approximately 0, with a standard deviation of 1. Several configurations were tried, including different combinations of activation functions, both for the hidden layers and final layer, loss functions and optimizers. Several feature inputs were also tested, and the best results appeared when the only features fed onto the networks were the ones utilized in the cuts presented on Tables VI and IX. An under sampling approach was taken, where due to the asymmetric amounts of data of signal versus background, a smaller subset of HS events was selected for training, with the remaining being used for validation alone. With this said, 70% of the background events was selected for training the NN, alongside a comparable signal sample.

Due to the inherent randomness of ML algorithms, several configurations were tested. Additionally, networks with the exact same characteristics were also trained several times. From these tests, the NN that showed the best selection efficiency for the HS signal, while removing all of the background events, was chosen as the best one. In order to remove all of the background events, we determined the selection threshold to be equal to the maximum score obtained by a background event, maintaining the 0 background criterion set in the kinematic cuts. Binary selection NNs provided the best results. Apart from this, no single NN configuration consistently showed better performances. The selected NNs had from 2 to 3 hidden layers, and the number of nodes per layer varied from 30 to 10. After the best NNs for each sample were selected, we obtained the final selection efficiencies for every sample by passing the events through all the NNs that relate to same background, and selecting as true positives any events that were given as signal by at least one of these NNs (e.g. if we are selecting an event of $N \to e^{\mp}\pi^{\pm}$, all NNs trained on HNL data sets score the event, and if at least one score is above the threshold given for the respective network, the event is considered a positive).

A summary of the results obtained by applying machine learning methods to our samples is shown in Table XI.

Comparing the selection efficiencies obtained with the standard kinematic cuts, presented in Table X, with the ones obtained by using machine learning algorithms in Table XI, we can clearly see that there is a improvement when NNs are involved in the analysis. All samples show higher efficiencies, regardless of whether there is missing

Sample	Signal Events Selected (%)	Signal Events in the Final Selection (%)
$N \to e^-\pi^+$	22467 (89.5)	23098 (92.0)
$N \to \mu^-\pi^+$	25825 (96.1)	26077 (97.1)
$N \to e^-\rho^+$	9847 (44.9)	13558 (61.8)
$N \to \mu^-\rho^+$	10817 (44.6)	15528 (64.1)
$N \to \nu_\alpha\mu^+\mu^-$	11875 (41.0)	14855 (51.2)
$N \to \nu_\alpha\rho^0$	14303 (66.9)	15225 (71.2)
$A' \to e^-e^+$	29061 (87.2)	30216 (90.7)
$A' \to \mu^-\mu^+$	16608 (98.0)	16698 (98.5)
$*A' \to e^-e^+$	N.A.	27274 (90.3)
$*A' \to \mu^-\mu^+$	N.A.	13704 (98.3)

TABLE XI. Summary of the results obtained by the chosen Neural Networks, discriminated by the samples they were trained with. The final selection efficiencies are obtained by applying all the NNs that share the same background as the sample. *Samples within the most recent sensitivity estimates. For these only the final selection efficiency is shown, since these data sets were not used to train any NN and as such N.A. stands for Not Applicable.

energy or not in the decay.

The samples that receive a smaller boost in their selection efficiency are the ones where usually there is no energy missing in their reconstructions, such as the DPs and the HNL decays that involve charged leptons accompanied by charged pions ($N \to \ell^\mp\pi^\pm$), which range from an extra 3.2% to 10.7% for the selection of $A' \to \mu^-\mu^+$, within the most recent sensitivity limits, and $N \to e^-\pi^+$ events respectively. On the other hand, HNL samples involving decays with missing energy had surprisingly good selection efficiencies, even more so when compared to the standard kinematic cuts. The selection of HNL events that decay to a SM neutrino and a pair of muons received an astounding increase of 47.6%, and the selection of events that decay to a neutral rho meson alongside a SM neutrino got an even more impressive increase of 64.6%, clearly showcasing the benefit of using machine learning methods in studies such as these.

The SHAP software [28] was utilized in order to interpret the relative importance given by the NNs to every feature fed onto it. It utilizes an approach based on the Shapley value [29] that estimates the relative contribution of each feature into the final score provided by the network, for each event, and is able to show the mean contributions per feature, for a data set. The SHAP analysis showed that the Impact Parameter was indeed a very influential factor, ranking top two or three for every NN trained on an HNL sample. A rather surprising result was that the Total Momentum of the reconstructed HS candidate particle was always the most significant feature. Nevertheless, we were also able to visualize the SHAP values attributed to each feature vs said feature for each individual event, and it became clear that the selection provided by NNs can never be replicated through cut-based approaches, and as such the most relevant feature for a network might not be the same when using other methods.

VII. STUDIES ON REDUCED VACUUM

The decay vessel is $\approx$ 50 m-long, and is currently planned to be set at a pressure of 1 mbar in order to minimize neutrino DIS interactions that would contribute to the background. However, at the start of data-taking some conditions may not be met. Additionally maintaining any level of vacuum on such a big volume is costly, and if the pressure was to be set at atmospheric levels of 1 bar a lot of money could be saved. However, this is only viable if the sensitivity to the HS particles is not compromised. To verify whether the sensitivities are influenced by the air pressure and if this extreme scenario is possible, we performed a similar study to the one done previously, but the decay vessel was set at an air pressure of 1 bar. All of the HS samples were generated again, with the same parameters set in Section IV, but were propagated through the apparatus in the new conditions. Since the neutrino DIS background was the hardest to remove through ML methods, we disregarded the muon DIS background, and generated 1.0×10^6 electron and muon flavoured neutrino and anti-neutrino events forced to interact within the same limits as previously. A summary of the new samples generated is shown in Table XII.

Sample	Events Generated	Particles Reconstructed (inside the Decay Vessel)
$N \to e^-\pi^+$	1.2×10^5	26709 (26181)
$N \to \mu^-\pi^+$	1.2×10^5	27006 (26676)
$N \to e^-\rho^+$	9.0×10^4	25286 (22203)
$N \to \mu^-\rho^+$	9.0×10^4	27674 (24526)
$N \to \nu_\alpha\mu^+\mu^-$	1.2×10^5	28671 (28660)
$N \to \nu_\alpha\rho^0$	9.0×10^4	21428 (21074)
$A' \to e^-e^+$	1.25×10^5	37024 (34982)
$A' \to \mu^-\mu^+$	5.0×10^4	17557 (16746)
$*A' \to e^-e^+$	1.15×10^5	33508 (31632)
$*A' \to \mu^-\mu^+$	4.0×10^4	14496 (13781)
ν_e DIS	1.0×10^6	129329 (96975)
$\overline{\nu_e}$ DIS	1.0×10^6	74777 (54523)
ν_μ DIS	1.0×10^6	31376 (24068)
$\overline{\nu_\mu}$ DIS	1.0×10^6	20988 (16202)

TABLE XII. Summary of all the samples generated with the **FairShip** software with a decay vessel set at a pressure of 1 bar. *Dark Photon samples without the events with masses of 3.6 and 4.4 GeV/c^2, which are not within the most recent sensitivity studies.

A. Cut-Based Study

The first step in analysing whether or not the new conditions were viable was to compare the results obtained when applying the kinematic cuts established in Tables VI and IX on the new samples. Table XIII shows the final efficiencies obtained by sample.

Sample	Surviving Events after the Cuts (%)
$N \to e^- \pi^+$	13516 (51.6)
$N \to \mu^- \pi^+$	23231 (87.1)
$N \to e^- \rho^+$	5002 (22.5)
$N \to \mu^- \rho^+$	7418 (30.3)
$N \to \nu_\alpha \mu^+ \mu^-$	1092 (5.2)
$N \to \nu_\alpha \rho^0$	1351 (4.7)
$A' \to e^- e^+$	27981 (80.0)
$A' \to \mu^- \mu^+$	16101 (96.2)
$*A' \to e^- e^+$	25608 (81.0)
$*A' \to \mu^- \mu^+$	13253 (96.2)
HNL Background	107 (0.1)
DP Background	55 (0.0)

TABLE XIII. Summary of the selection efficiency obtained by applying the kinematic cuts from Section V on their corresponding samples. All the efficiencies are relative to the HS candidate particles reconstructed within the decay vessel. *Dark Photon events without the 3.6 and 4.4 GeV/c^2 mass samples, that are not within the most recent sensitivity estimates.

Comparing the data from Table XIII with the one from Table X, we can clearly see that all the HS samples with decays involving electrons have lost significant amounts of their selection efficiency. From these, the HNL samples have suffered the most, with both decays involving electrons losing about one third of their selection efficiency, with a drop from 81% to 52% and 36% to 20%, for the pion and rho decays respectively. On the other hand, samples that involve decays to muons do not show a clear tendency, because even though the HNL samples with semi-leptonic decays have slight decreases in selection efficiency, the HNL and DP samples that lead to the detection of muon pairs actually show an increase, even though it is only a net gain of around 1%.

The first phenomenon was anticipated, since now that the Decay Vessel is filled with air, the electrons resulting from decays of the HS particles will interact much more. While this does not necessarily lead to a sizeable decrease in the number of reconstructed particles, as can be seen from Table XII, the increasing number of interactions leads to a much bigger energy loss by the electrons, immediately skewing the Impact Parameter of the reconstructed particle. Since pions do not radiate as much as the electrons, due to their mass, an asymmetric momentum loss appears, increasing the Impact Parameter, which is the main selection criterion for our analysis. This is further corroborated by the much smaller decrease in selection efficiency of the DP to an electron pair sample of just 4%, since the momentum loss is now more symmetrical. As for the increase in the selection efficiency of some samples, we cannot see a fundamental reason as to why this should happen, besides inherent statistical fluctuations.

The last noteworthy takeaway from Table XIII is that due to the surviving background events the previous kinematic cuts are no longer reasonable, since the number of expected background events for a vessel at atmospheric pressure is bigger than for one in vacuum, and as such for the background levels to stay the same, the number of these events that pass through the selection criteria should be at least the same. In order to remove every single background event for the HNLs, 16 cuts that tightened the conditions on the ones already established in Table VI were needed, and as for the DPs, 10 were needed, that also increased the constraints, when compared to those in Table IX. The final selection efficiencies obtained for 0 background events selected through the new filters are shown in Table XIV. As expected, all selection efficiencies worsened drastically.

Decay Mode	Surviving Events after the Cuts (%)
$N \to e^- \pi^+$	7046 (26.9)
$N \to \mu^- \pi^+$	15710 (58.9)
$N \to e^- \rho^+$	2676 (12.1)
$N \to \mu^- \rho^+$	4441 (18.1)
$N \to \nu_\alpha \mu^+ \mu^-$	396 (1.4)
$N \to \nu_\alpha \rho^0$	620 (2.9)
$A' \to e^- e^+$	18983 (54.3)
$A' \to \mu^- \mu^+$	13504 (80.6)
$*A' \to e^- e^+$	17433 (55.1)
$*A' \to \mu^- \mu^+$	11070 (80.3)

TABLE XIV. Summary of the selection efficiency obtained by applying the kinematic cuts that remove all background events for both HNLs and DPs, detailed by decay mode.

B. Machine Learning

In an attempt to improve the selection efficiencies obtained on the 1 bar setup, machine learning methods were applied to distinguish the HS signal from the background. Following a similar procedure to that of Section VI, we obtained the results summarized in Table XV.

Comparing the results shown in Table XV with those in Table XIV, most of the selection efficiencies were improved. The only outlier was the $N \to \mu^- \pi^+$ sample, where the efficiency dropped. However, this is probably an artifact of our 0 background events selected cri-

Sample	Signal Events Selected (%)	Signal Events in the Final Selection (%)
$N \to e^-\pi^+$	6249 (23.9)	7849 (30.0)
$N \to \mu^-\pi^+$	8047 (30.2)	12113 (45.4)
$N \to e^-\rho^+$	3123 (14.1)	5120 (23.1)
$N \to \mu^-\rho^+$	5356 (21.8)	6663 (27.2)
$N \to \nu_\alpha\mu^+\mu^-$	757 (2.6)	1497 (7.6)
$N \to \nu_\alpha\rho^0$	927 (4.4)	1611 (5.2)
$A' \to e^-e^+$	14694 (42.0)	18062 (51.6)
$A' \to \mu^-\mu^+$	14010 (79.8)	14342 (85.6)
$*A' \to e^-e^+$	N.A.	15656 (49.5)
$*A' \to \mu^-\mu^+$	N.A.	11501 (83.5)

TABLE XV. Summary of the results obtained by the NNs that provided the best selection efficiencies for 0 background events selected. *Samples within the most recent sensitivity estimates. N.A. stands for Not Applicable, since no NNs were trained on these samples.

terion, since NNs provide near-optimal solutions based on local minimums of loss-functions, and the increase in fringe background events makes finding a global minimum much more volatile, and thus the weights that provide lower scores to these fringe events harder. Nevertheless, no selection efficiencies were satisfying besides for the $A' \to \mu^-\mu^+$ sample.

VIII. CONCLUDING REMARKS

In this thesis we provide several optimized background veto criteria for the search of HNLs and DPs based on the kinematic properties of the reconstructed particles, around the regions of expected sensitivity. We present a kinematic cut-based approach that explores, in particular, the discriminating power of the Impact Parameter to remove all background events while obtaining selection efficiencies above 80% for both the $N \to \ell^\mp\pi^\pm$ and $A' \to \ell^-\ell^+$ samples. The samples where the reconstructions had missing energy, however, had poor selection efficiencies, of less than 7%. With the introduction of machine learning methods, we are able to enhance said efficiencies further, reaching over 97% for the $N \to \mu^\mp\pi^\pm$ and $A' \to \mu^-\mu^+$ samples. The missing energy samples were the most improved with new selection efficiencies of over 51%.

Having established satisfying selection efficiencies for standard detector conditions, we proceeded to verify whether the Decay Vessel vacuum conditions could be relaxed. It became apparent that the new conditions heavily degrade the selection efficiencies of the HS particles, even if we assume that the expected background events stay the same. We conclude accordingly that the extreme scenario where the SHiP experiment would be conducted at atmospheric pressure (in place of the standard vacuum conditions foreseen) would result in drastic losses in sensitivity, and thus should not be viable.

[1] A. Buonaura, *Journal of Physics: Conference Series* **1586**, 012031 (2020).
[2] SHiP Collaboration, A facility to Search for Hidden Particles (SHiP) at the CERN SPS (2015).
[3] P. Minkowski, *Physics Letters B* **67**, 421 (1977).
[4] L. Okun, *Sov. Phys. JETP* **56**, 502 (1982).
[5] M. Shaposhnikov, *Nuclear Physics B* **763**, 49–59 (2007).
[6] E. Goudzovski, *EPJ Web of Conferences* **96**, 01017 (2015).
[7] T. Asaka, M. Shaposhnikov, *Physics Letters B* **620**, 17 (2005).
[8] B. Pontecorvo, *Sov. Phys. JETP* **26**, 984 (1968).
[9] T. Asaka, M. Shaposhnikov, M. Laine, *Journal of High Energy Physics* **2007**, 091–091 (2007).
[10] P. Langacker, *Rev. Mod. Phys.* **81**, 1199 (2009).
[11] B. Holdom, *Physics Letters B* **166**, 196 (1986).
[12] T. Sjöstrand, S. Mrenna, P. Skands, *Computer Physics Communications* **178**, 852–867 (2008).
[13] C. Andreopoulos, *et al.*, *Nuclear Instruments and Methods in Physics Research Section A: Accelerators, Spectrometers, Detectors and Associated Equipment* **614**, 87–104 (2010).
[14] T. Sjöstrand, S. Mrenna, P. Skands, *Journal of High Energy Physics* **2006**, 026–026 (2006).
[15] SHiP Collaboration (2015).
[16] S. Agostinelli, *et al.*, *Nucl. Instrum. Meth. A* **506**, 250 (2003).
[17] M. Al-Turany, *et al.*, *Journal of Physics: Conference Series* **396**, 022001 (2012).
[18] E. Van Herwijnen, H. Dijkstra, M. Ferro-Luzzi, T. Ruf (2015).
[19] B. Hosseini, W. M. Bonivento (2017).
[20] SHiP Collaboration, Sensitivity of the ship experiment to heavy neutral leptons (2019).
[21] SHiP Collaboration, Sensitivity of the ship experiment to dark photons decaying to a pair of charged particles (2020).
[22] W. Altmannshofer, S. Gori, M. Pospelov, I. Yavin, *Physical Review D* **89** (2014).
[23] W. Altmannshofer, S. Gori, M. Pospelov, I. Yavin, *Physical Review Letters* **113** (2014).
[24] SHiP Collaboration, SHiP Experiment - Comprehensive Design Study report, *Tech. Rep. CERN-SPSC-2019-049. SPSC-SR-263*, CERN, Geneva (2019).
[25] P. C. Bhat (2010).
[26] F. Chollet, *et al.*, Keras, `https://github.com/fchollet/keras` (2015).
[27] M. Abadi, *et al.*, TensorFlow: Large-scale machine learning on heterogeneous systems (2015). Software available from tensorflow.org.
[28] S. Lundberg, S.-I. Lee, A unified approach to interpreting model predictions (2017).
[29] L. S. Shapley, *Notes on the n-Person Game —II: The Value of an n-Person Game* (RAND Corporation, Santa Monica, CA, 1951).